

# Implementation of a spherical double plasma-mirror telescope for a multi-Petawatt laser

V. SCUTELNIC,<sup>1,‡,\*</sup> M. SPEICHER,<sup>1,‡</sup> A. FAZZINI,<sup>1</sup> P. GHENUCHE,<sup>2</sup> D. DORIA,<sup>2</sup> A. AILINCUTEI,<sup>3</sup> B. GONZALEZ- IZQUIERDO,<sup>1</sup> T. ASAVEI,<sup>2</sup> S. BALASCUTA,<sup>2</sup> J.J. BEKX,<sup>1</sup> P.-G. BLEOTU,<sup>2</sup> G. BODINI,<sup>1</sup> C. BRAGANZA,<sup>1</sup> A. F. BRODERSEN,<sup>1</sup> A. CAVALLI,<sup>1</sup> O. CHALUS,<sup>3</sup> G. COJOCARU,<sup>2</sup> J. D'MELLO,<sup>1</sup> I. DANCUS,<sup>2</sup> C. DERYCKE,<sup>3</sup> F. DEURVORST,<sup>1</sup> M. EHREMANNTAUT,<sup>1</sup> D. GENGENBACH,<sup>1</sup> D.G. GHITA,<sup>2</sup> L. GIUFFRIDA,<sup>4</sup> M. GUGIU,<sup>2</sup> M. M. GÜNTHER,<sup>1</sup> O. JUINA,<sup>1</sup> K. KENNEY,<sup>1</sup> S. KUMAR,<sup>1</sup> M. MARTINEZ-PACHECO,<sup>1</sup> I. MINGUEZ BACHO,<sup>1</sup> S. NORBAEV,<sup>2</sup> N. POETRANTO,<sup>1</sup> H. RUHL,<sup>1</sup> E. SCHORK,<sup>1</sup> M. STEIN,<sup>1</sup> S. STEINKE,<sup>1,¶</sup> A.-M. TALPOSI,<sup>2</sup> A. TOMA,<sup>2</sup> M. TOSCA,<sup>4,5</sup> A. UBARHANDE,<sup>1</sup> L. VASESCU,<sup>2</sup> E. GAUL,<sup>1</sup> D. E. RIVAS,<sup>1</sup> M. S. SCHOLLMEIER,<sup>1,¶</sup> AND G. KORN<sup>1</sup>

<sup>1</sup>Marvel Fusion GmbH, Theresienhöhe 12, 80339 Munich, Germany

<sup>2</sup>Extreme Light Infrastructure (ELI-NP) & Horia Hulubei National Institute for R&D in Physics and Nuclear Engineering (IFIN-HH), 30 Reactorului Street, 077125 Magurele, Romania

<sup>3</sup>Thales LAS France, 78990 Élanecourt, France

<sup>4</sup>ELI Beamlines Facility, The Extreme Light Infrastructure ERIC, Dolní Brežany 252 41, Czech Republic

<sup>5</sup>Charles University, Faculty of Mathematics and Physics, Department of Macromolecular Physics, Prague 180 00, Czech Republic.

<sup>‡</sup>These authors contributed equally

<sup>¶</sup>Until June 2023

\*[valeriu.scutelnice@marvellfusion.com](mailto:valeriu.scutelnice@marvellfusion.com)

<sup>¶</sup>[marius.schollmeier@marvellfusion.com](mailto:marius.schollmeier@marvellfusion.com)

**Abstract:** High-power laser beamlines typically operate with fixed focusing conditions, limiting the achievable focal spot size and, consequently, the peak intensity at the focus. To mitigate these restrictions, prior studies explored the use of curved plasma mirrors for F-number change to a specific value. Here, a double plasma-mirror (DPM) system including spherical optics in a telescope configuration is implemented to adapt the F-number of a multi-Petawatt (PW) laser beam resulting in adjustability within a range of intensities. The system is optimized to minimize aberrations at the focal plane, which ensures a high-quality focal spot. A dedicated imaging system is used to evaluate focus quality and to measure the total reflectivity of the DPM configuration at the multi-PW-level. Temporal contrast enhancement of the reflected beam is additionally demonstrated, as evidenced by higher particle yield and increased maximum kinetic energy of accelerated proton beams from nanometer-thick foils, compared to results without DPM. These findings enable the exploration of more extreme laser-plasma conditions in multi-PW laser facilities that require ultra-high temporal contrast and intensity, while also expanding the capabilities of high-power laser facilities by enabling intensity adjustment to levels beyond their designed specifications.

## 1. Introduction

High-power short-pulse lasers open new horizons in laser-plasma physics. In addition to being routinely used for particle acceleration [1-4], they have also been deemed to be a plausible path to fusion [5, 6]. This class of laser facilities utilizes beamlines with fixed F-number of the final focusing optic, which usually represents an off-axis parabolic mirror or a spherical mirror for producing an aberration-free, diffraction-limited focus. Such optics have high fabrication costs

associated with their specialized optical characteristics (such as surface roughness, surface figure, coating uniformity, surface and coating defects) across a large (sub-meter-size) clear aperture. Extending the tunability range of intensity at the laser focus broadens the range of intensity-dependent phenomena that can be investigated at the same beamline. For a beamline with a fixed F-number, the intensity achievable at the laser focus can be primarily adjusted by controlling the pulse duration and pulse energy. However, temporally stretching the pulse or reducing the energy results in lower intensities at the focus and might be detrimental for the process under investigation.

Alternatively, an adjustable intensity at the laser focal plane can be achieved by changing the F-number of the beam after the final focusing optic while keeping the pulse duration and energy constant. Traditionally, this approach relies on curved plasma mirrors (PM)—transparent optics that are inserted in the vicinity of the final focus, where the laser at high fluence ignites a reflective plasma sheath on the optics' surface [7]. As first shown by Gold *et al.* on flat substrates [8], the plasma reflectivity can be high, while the spatial profile of the reflected beam is smooth. Moreover, the generated plasma acts as a self-induced temporal shutter (Kapteyn *et al.* [9]), leading to numerous applications of plasma mirrors for temporal contrast improvement of the laser pulse [10–24]. Temporal contrast is recognized as a critical parameter for efficient laser interaction with nanometer-thick solid targets, as for example demonstrated in [25].

The application of curved plasma mirror substrates to refocus the laser beam to a smaller F-number has been initially proposed by Nakatsutsumi *et al.* [26], where an ellipsoidal plasma mirror made of glass with an antireflective surface coating was used to reach higher intensities [27]. However, glass ellipsoidal mirrors are difficult to polish due to the complex surface geometry preventing scalability of mass production and making them expensive. Wilson *et al.* [28] advanced this method by implementing an approach of producing plastic ellipsoidal plasma mirrors by casting a plastic ellipsoid from a computer numerical control (CNC) machined metal mold. Yet, the plastic mirrors are impaired by reduced surface quality after the casting process. Another example of curved optics is the use of a single spherical plasma mirror by Kojima *et al.* [29] to refocus the laser beam in the target chamber, although to avoid introducing aberrations the F-number of the beam needs to be constant and the angle of incidence on the mirror is limited to the range of  $0^\circ$ – $0.5^\circ$ . A theoretical study using an off-axis parabolic plasma mirror to change the F-number of a tightly focused beam was recently published by Geng *et al.* [30] in the context of laser-electron acceleration. All these examples utilize optics with tight curvatures (focal length of  $\sim 3$  mm in [27] and  $< 1$  mm in [30]), which poses unique challenges to the design and application of the antireflective coating across the surface due to the large range of incidence angles and broad bandwidth of short-pulse laser beams. This limitation further constrains the broader use of curved plasma mirror optics for F-number adjustments. To overcome the limitations mentioned above, we consider optical systems in which the beam is reflected between two or more curved optical elements without being obscured by the reflecting optics, referred to as “unobscured optical systems”. Outside the field of high-power lasers, imaging with unobscured optical systems consisting of two spherical mirrors has been largely implemented in telescopic instrumentation, where nearly diffraction-limited image quality has been achieved. Optimal configurations for the spherical mirrors can be chosen based on third-order aberration theory. As one particular example, A. Kutter developed the Schiefspiegler telescope [31] having an unobscured optical configuration with two spherical mirrors, while A.S. Leonard further implemented aspheric modifications in Yolo telescopes that allowed for a better correction of the astigmatism [32].

Here, we build on the approach of using two spherical glass substrates to design and implement a double plasma-mirror (DPM) telescope for both adjusting the F-number, and hence the intensity at focus, and enhance the temporal contrast of a large-aperture, multi-Petawatt (PW) laser system. The configuration of the mirrors is chosen such that the aberrations from the two surfaces are nearly cancelled out, allowing for a rather large angle of incidence

on the spherical mirrors while the distribution of incidence angles across the beam aperture stays narrow to effectively utilize the antireflective coating for contrast enhancement. Furthermore, the system's design ensures low sensitivity to misalignment, allowing for intensity adjustment simply by changing the distances in the optical system, unlike systems that rely on higher-order optical surfaces. A custom-designed, high-power imaging diagnostic was implemented to validate the spatial energy distribution and peak intensity at the laser pulse focus, with a total energy of 188 J and 24 fs in duration (7.8 PW) delivered to the target chamber, and to evaluate the total reflectivity of the DPM system at such high energies. Additionally, enhancement of the temporal intensity contrast of the multi-PW laser beam is confirmed by the higher particle yield and increased cut-off kinetic energy of laser-driven proton beams from nanometer-thick flat foils, compared to a system without contrast-enhancing plasma mirrors.

## **2. Double plasma-mirror setup and high-power diagnostic**

### *2.1 Configuration of the double plasma-mirror system*

The spherical DPM system was implemented at the 10 PW long-focus beamline at Extreme Light Infrastructure – Nuclear Physics (ELI-NP). Linearly polarized laser pulses at 810 nm central wavelength with  $24 \pm 1$  fs (full width at half maximum, FWHM) pulse duration, with energy up to 188 J, and a beam diameter of 48 cm are primarily focused by a F/63.5 on-axis spherical mirror with a focal length of 30.5 m [33]. The focused beam subsequently passes through a central hole in the final turning mirror, located before the focusing spherical mirror, to reach the target chamber (Figure 1a). This results in the low-energy F/63.5 focal spot depicted in Figure 1b, as measured by an imaging system located downstream the focal plane. The implemented DPM system is positioned near the focal plane of the F/63.5 focusing mirror, forming a telescope with a pair of spherical glass substrates that reflect the beam in the vertical plane, resulting in a F/19.4 focus, as shown in Figure 1a. In this configuration, the first mirror of the system, PM1, exhibits a convex front surface with a radius of curvature of 155 mm, while the second mirror, PM2, exhibits a concave front surface with a radius of curvature of 103.7 mm. PM1 is placed 178 mm upstream the F/63.5 focal plane. PM1 and PM2 are separated by 43.5 mm and the angle of incidence is fixed at  $7^\circ$  on each plasma mirror. The resulting focal plane is located 73 mm from PM2, ensuring sufficient clearance for positioning of samples to be irradiated at the focus. Commercial off-the-shelf spherical lenses were selected for plasma mirror substrates due to their high optical quality and availability in large quantities. An antireflective coating ( $0.3 \pm 0.05\%$  reflectivity between 760-860 nm) is applied on both surfaces of the plasma mirrors to minimize the reflection of any preceding signal and potential pre-pulses prior to the main laser peak. The antireflective coating on the back surface facilitates additionally the alignment of the plasma mirrors in the presence of multiple reflections caused by the rear surfaces (see Section 2.1 of SI).

Likewise, the DPM system was positioned to ensure that the s-polarized beam [34] has a diameter of 2.6 mm on the first mirror, leading to laser intensities in the range of  $10^{16}$ - $10^{17}$  W/cm<sup>2</sup> (Section 2.2 of SI). These intensities are required to ensure maximum reflectivity, as shown by Ziener *et al.* [10]. Moreover, for such peak intensities and given the measured temporal intensity contrast of the incoming laser beam,  $<10^{-7}$  at -5 ps (see ref. [35] and Figure S4 of SI), the preceding signal lacks sufficient intensity to initiate plasma formation. As a result, this preceding signal passes through the mirrors of the DPM system, enhancing the temporal intensity contrast in the process.

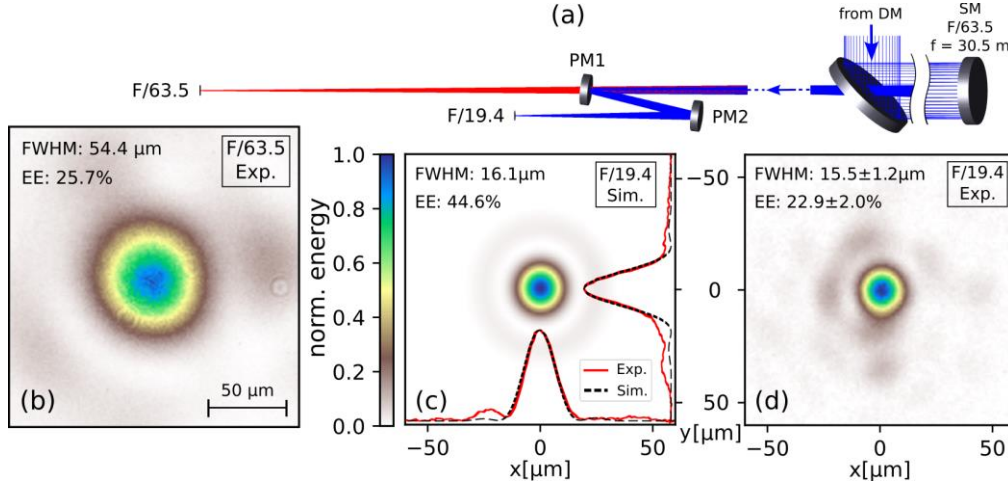


Fig. 1. (a) Laser beam delivery and double plasma-mirror (DPM) configuration implemented at ELI-NP. PM1: convex plasma mirror 1; PM2: concave plasma mirror 2. A deformable mirror, DM, located at the compressor enables fine adjustment of the focus. An F/63.5 spherical mirror, SM, focuses the laser through the routing hole in the last turning mirror into the target chamber. The F/63.5 laser beam is s-polarized on the plasma mirrors impinging at  $7^\circ$  angle of incidence. The plasma mirror substrates were AR coated on both front and back surfaces. (b) Experimental focus of the F/63.5 beam as measured in a downstream microscope. (c) Simulated focus of the resulting F/19.4 with deformable mirror correction and (d) the corresponding experimental focus as measured in the downstream microscope. FWHM: full width at half maximum of the focus; EE: encircled energy within FWHM. Inset in (c) is horizontal and vertical lineouts of the simulated and experimental foci. See Section 4 of SI for details on the focus image analysis and background treatment.

Ray-tracing simulations using OpticStudio by Zemax (Ansys) provide an estimate of the aberrations for the DPM configuration described above (see Figure S5a,b in SI). Simulations anticipate that the focus after the DPM system preserves the majority of the energy around the central region, as shown by a theoretical Strehl ratio reaching 0.776. The wings are an order of magnitude lower in intensity than the central peak and are dominated by vertical astigmatism, which can be corrected by the deformable mirror located upstream in the laser beamline. Additionally, a moderate flexing of the deformable mirror membrane in the range of  $\pm 210$  nm is sufficient to reduce this aberration (see Section 2.4 of SI). The resulting simulated focus after deformable mirror correction is shown in Figure 1c.

Experimentally, a microscope located downstream from the focal plane images the resulting focus at low energy. Figure 1d illustrates a representative image of the measured energy distribution at the focal plane. The microscope is constructed with a 5x objective (Mitutoyo) and a tube lens with a resulting numerical aperture of 0.14, thereby inducing negligible aberrations to the measured focus. As anticipated, the DPM system introduced low-order residual astigmatism, which was effectively corrected using the deformable mirror as described in Section 2.4 of SI. Those minimal aberrations in the measured F/19.4 focal spot are evident from the horizontal and vertical lineouts when compared to the simulated focal spot (inset in Figure 1c). Consequently, the experimentally measured focus exhibits a diameter of  $(15.5 \pm 1.2)$   $\mu$ m (FWHM), in line with the expected value from simulations, while ensuring an encircled energy of  $22.9 \pm 2\%$ . The similarity of the encircled energy measured in the DPM F/19.4 focus with the original F/63.5 focus (25.7%) indicates that two factors may contribute to the reduction of the encircled energy compared to the ideal case (50%): presence of higher-order Zernike terms that could not be corrected with the deformable mirror, and the optical power spectral density of the spherical focusing mirror that contributes to the scattering of light in the vicinity of the focus.

Notably, the same set of plasma mirrors can be used to continuously adjust the beam F-number for additional intensity control and tailoring the focal spot size. In the configurations described in Section 2.5 of SI, the beam's F-number is adapted from F/30 to F/16 by adjusting concomitantly the distance from PM2 to the resulting focal plane and PM1 to the original focal plane (see Figure 1a). The results indicate that reducing the F-number increases the laser intensity at the focal point and decreases the focal spot size, although this also significantly enhances astigmatic aberrations when approaching F/16. Conversely, larger F-numbers effectively reduce aberrations while reducing the focal intensity and enlarging the focal spot size. For F-numbers exceeding F/30, the intensity at PM1 surpasses the optimum level for maximizing plasma reflectivity, which further reduces the focal intensity and compromises the effectiveness of the temporal intensity contrast enhancement. A F/19.4 configuration was therefore identified as the optimal setup, achieving the highest focal-plane peak intensity with minimal aberrations while maximizing the temporal intensity contrast enhancement. The capabilities of the double plasma-mirror telescope can be expanded by altering the laser beam properties or adjusting the curvature radius of the optical components within the system.

## *2.2 Laser focus characterization at high power*

A dedicated on-shot imaging diagnostic, operating at high energies, was designed and implemented to additionally assess laser focus quality at Petawatt levels, and evaluate the effects of plasma formed on the surface of the mirrors of the DPM system at increasing intensities. This high-power diagnostic (HPD), depicted in Figure 2a (and a detailed layout included in Figure S13 in SI), is designed to attenuate and image the focus of a 10 PW laser beam at full energy and is used with  $\sim 175$  J total energy and  $\sim 24$  fs in duration in this investigation. Following the DPM system, the high-energy beam propagates in vacuum to an uncoated, concave parabolic mirror with 30.5 cm diameter and 2.54 m focal length. The concave mirror is at an incidence angle of  $0.25^\circ$  and reimages the focus in the vicinity of the incoming beam's focal plane. Two uncoated wedges are used to reduce the energy of the beam before a 4f telescope (1.52 m focal length lenses, aperture 102 mm, F/14.9) that relays the intermediate focus onto an optical table outside the vacuum chamber. The uncoated optics provide 5 orders of magnitude attenuation to the first lens of the 4f telescope, while the beam passes collimated through the vacuum window. The low fluence ( $< 0.07$  mJ/cm<sup>2</sup>) along the vacuum window, as well as low B-integral ( $< 0.22$ ) minimize any unwanted nonlinear effects and other distortions of the image. On the outside optical table, a 5x microscope ultimately images the relay-imaged focus to a CMOS detector. The routing mirrors on the outside optical table are silver-coated excepting one that is replaced with an uncoated wedge to achieve a total attenuation of 7 orders of magnitude at the entrance of the 5x microscope. Further attenuation on the detector is achieved via neutral density filters.

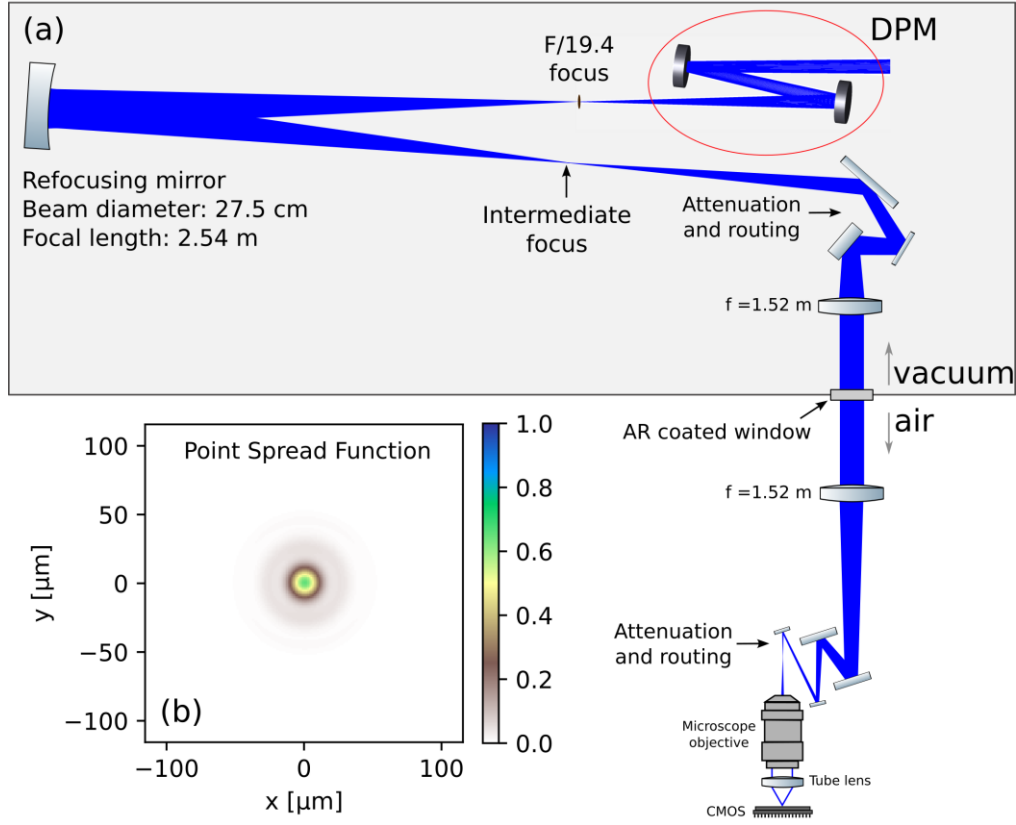


Fig. 2. (a) High-power diagnostics layout to image the focus produced by the DPM telescope (red ellipse) during a high-power laser shot up to 10 PW. After the final focus, the beam is first propagated to a large refocusing on-axis parabolic mirror (left) until the intensity is low enough to reflect a small fraction of the laser without triggering a plasma on the optic surface. The reflected light is brought to an intermediate focus next to the incoming beam. The intermediate focus is relay-imaged to a microscope outside the target chamber with a  $4f$  telescope. Before the first lens, the beam is attenuated using two uncoated wedges such that a parallel beam with about three-inch diameter can safely propagate through the vacuum window. Outside the vacuum, the beam is attenuated across one uncoated wedge and several routing mirrors. Finally, a  $5\times$  microscope, similar to the in-chamber downstream microscope, is used to record the focal spot image on shot. The laser beam is p-polarized on the optics of the high-power diagnostic, in contrast to the s-polarization on the DPM system. (b) Simulated Huygens Point Spread Function for the full spectral bandwidth of the laser showing high imaging quality, as confirmed by the simulated Strehl ratio of 0.65. For further details see the text and Section 5 of SI.

In order to estimate the imaging resolution of the HPD system, ray-tracing simulations have been performed (Figure 2b) using OpticStudio. From the calculated Strehl ratio, 0.65, it is anticipated that the measured peak intensity with the HPD system is 35% lower than the actual intensity achieved for the demagnified focus. The limited resolution of HPD is attributed to the aperture of the refocusing parabolic mirror and the chromatic aberrations in the relay lenses (see Section 4 of SI for further details) and was characterized with a USAF 1951 microscope calibration target placed at the focal plane of the F/19.4 beam.

The foci measured experimentally with the HPD system are shown in Figure 3. The system's performance was initially evaluated by imaging the focal spot at low energy, 20 mJ (Figure 3a). The peak intensity on PM1 resulting from this low energy was  $<2 \cdot 10^{11} \text{ W/cm}^2$ , which is below the trigger threshold of the DPM. Under these conditions, the focus covers a broader area [FWHM ( $24.6 \pm 1.2$ )  $\mu\text{m}$ ] and exhibits lower encircled energy [(17.4 $\pm$ 2)%]

compared to the focus measured in the target chamber (Figure 1d). The diminished focus quality can be explained by the limited resolution of the HPD system. Conversely, for an incoming laser light with high energy, 175 J, the intensity on the telescope mirrors reaches values of  $\sim 10^{16}$ - $10^{17}$  W/cm<sup>2</sup>, which are well above the threshold for plasma formation. In these high-energy conditions, the measured focal spot size using the HPD diagnostic (see Figure 3b) was  $(23.8 \pm 1.2)$   $\mu$ m, with an encircled energy of  $(15.3 \pm 2)$  %. These values are comparable to those measured at low energy, indicating that plasma formation on the telescope's mirrors induces minimal effects on the focus quality of the reflected laser light, as also evidenced from the horizontal (Figure 3c) and vertical (Figure 3d) lineouts relative to the measured low-energy focal spot.

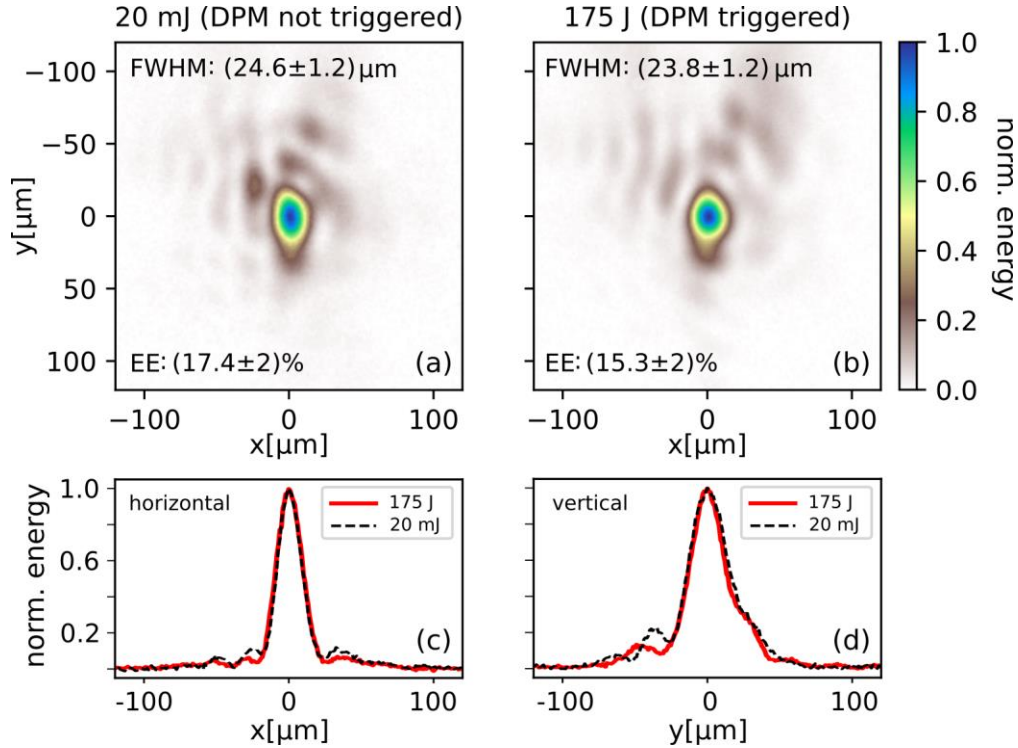


Fig. 3. (a) Foci measured with the high-power diagnostics at low energy, 20 mJ, and (b) high energy, 175 J. Close similarities of the normalized horizontal, (c), and vertical, (d), profiles along the center of both foci images demonstrate a minimal distortion of the focal spot when plasma is triggered on the mirror surfaces at high energy. Uncertainties are derived from the daily variation of the focus profile caused by deformable mirror settings and shot-to-shot fluctuation. FWHM: full width at half maximum of the focus; EE: encircled energy within FWHM.

The HPD configuration was additionally employed to characterize the total reflectivity of the DPM system. For this purpose, the signal in the focus image using the DPM system was integrated – following the background subtraction procedure detailed in Section 4 of SI – and then compared with the corresponding measurement taken without the DPM system. This analysis was conducted for laser intensities where efficient plasma formation is expected on the surface of the PM1 mirror, specifically for intensities ranging from  $6 \cdot 10^{16}$  W/cm<sup>2</sup> to  $1.4 \cdot 10^{17}$  W/cm<sup>2</sup>. The total reflected laser light by the DPM system, as shown in Figure 4, was measured to have an average value of  $(68 \pm 17)$  %, remaining relatively constant across the considered intensity range. These results are in line with previous works [10].



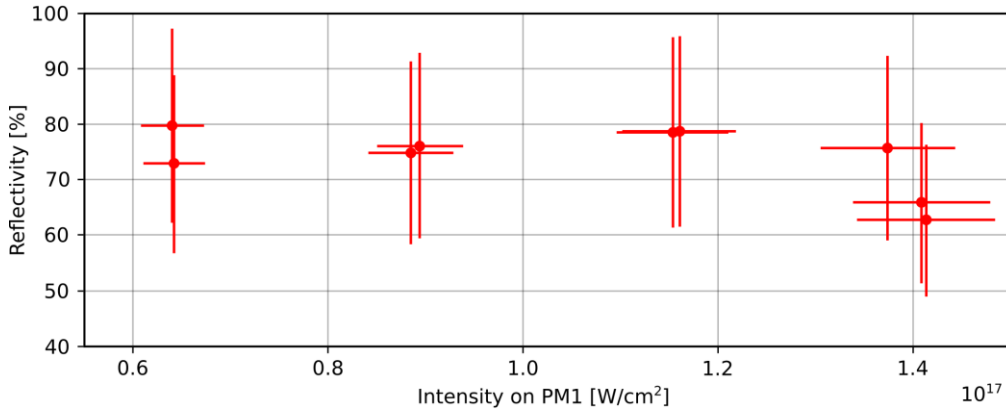


Fig. 4. Measured total reflected laser light on the DPM system as a function of the peak intensity on the first plasma mirror, PM1. Horizontal error bars (intensity on PM1 variation) are defined by the uncertainty in energy measurement at the laser diagnostic bench and pulse duration. Vertical error bars are defined by the uncertainties in microscope filter transmission to adapt the dynamic range, incoming energy, and energy calibration of the microscope camera.

Based on the focus size measured by a downstream microscope at low energy [ $(15.5 \pm 1.2)$   $\mu\text{m}$ , Figure 1d], along with the total DPM reflectivity [ $(68 \pm 17)$  %, Figure 4] and pulse duration [ $(24 \pm 1)$  fs, see Section 5 of SI], the resulting experimental intensity reaches a value of  $(8.7 \pm 2.5) \cdot 10^{20}$  W/cm $^2$ . This peak intensity is  $8.2 \pm 2.4$  times higher than what could be achieved under the same initial laser conditions without the DPM telescope system.

### 3. Characterization of the contrast enhancement

To characterize the on-target temporal intensity laser contrast, we examined proton acceleration from the interaction with thin planar foils. A laser pulse exhibiting low temporal intensity contrast is expected to pre-ionize the target and could diminish the coupling of the main laser beam energy into the pre-heated plasma, thereby reducing both the conversion efficiency to particle generation and the maximum kinetic energy of accelerated ion beams. Conversely, high contrast laser pulses prevent plasma expansion at an early stage of the laser-target interaction enabling efficient energy transfer of the laser beam to particle formation and motion [36]. This effect is particularly pronounced in nanometer-thick targets. To evaluate this, ultrathin planar carbon foils ( $\sim 5$  nm thick) were irradiated at a  $45^\circ$  incidence angle using high-energy laser pulses [ $(174 \pm 10)$  J before the DPM system]. The energy spectra of the accelerated proton beams were measured at specific discrete energies using a radiochromic film (RCF) stack placed approximately 50 mm downstream from the target and designed to capture the entire beam profile. Dedicated measurements were conducted using both the DPM system and an identically configured double-silver mirror (DSM) system. Silver mirrors were chosen for their high reflectivity at the laser wavelength (760-860 nm), enabling them to also reflect the preceding signals of the laser pulses. Therefore, the DSM system serves as a control case where the temporal intensity contrast of the reflected beam is expected to maintain similar values before and after reflection.

The measured proton spectra obtained using the DPM and DSM systems are shown in Figure 5. The total proton yield, conversion efficiency and maximum kinetic energy show a significant increase when using the DPM system compared to the DSM system (i.e., without enhanced laser contrast). Notice that even at this minimal target thickness, the DSM system generates a proton beam with energies up to 15 MeV, highlighting the inherently high contrast of the laser system. Conversely, in the case of the DPM system notably higher proton yield, conversion



efficiency and maximum kinetic energy are produced, generating proton energies exceeding 50 MeV (limited by the RCF stack, which was designed to detect proton energies only up to 50 MeV). These results provide evidence for a substantial enhancement of the temporal intensity contrast by the DPM system and demonstrate its feasibility for applications involving ultra-intense laser light and nanometer-scale solid targets.

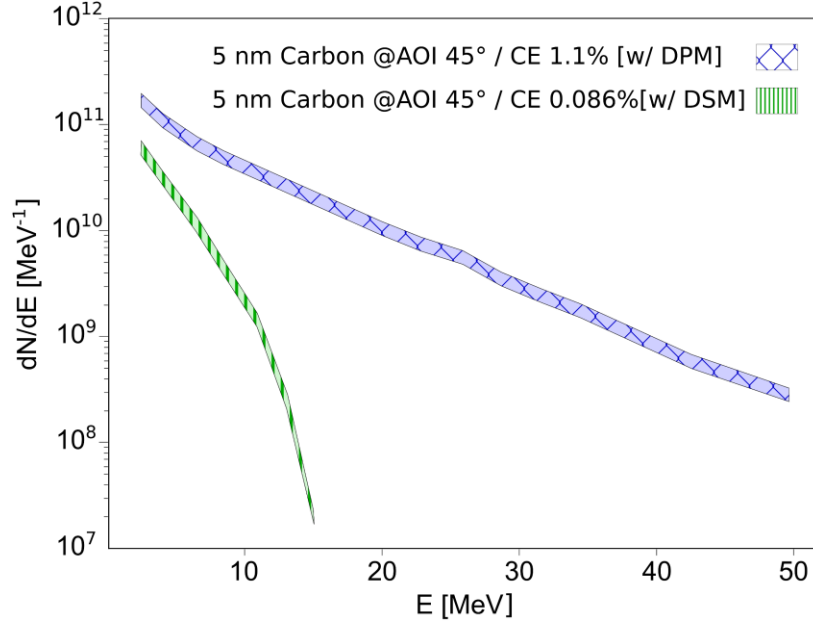


Fig. 5. Proton spectra from irradiated ~5 nm thick carbon foils, as calculated from the measured RCF data. Spectra with the DPM (blue mesh) and DSM systems (green stripes) reveal >50 MeV and ~15 MeV cut-off energies, respectively. The shaded areas correspond to the uncertainty in the calibration of the RCFs. The DPM system shows significantly higher cut-off energy, total particle number, and conversion efficiency (CE), highlighting a marked improvement in the temporal intensity contrast compared to the DSM case.

#### 4. Conclusion

A double-plasma-mirror (DPM) telescope system, using commercially available spherical optics, has been implemented and characterized for its ability to adjust intensity and to enhance temporal contrast in a multi-Petawatt laser beamline. A reduction from F/63.5 to F/19.4 with minimal aberrations at the image plane has been experimentally demonstrated. The aberrations introduced by each of the spherical mirror surfaces of the telescope system are compensating each other, resulting in a small astigmatism that is manageable by minor and predictable adjustment of a deformable mirror, as shown by measurements at low powers of the laser.

The focus quality at high energy levels was evaluated using an imaging system diagnostic with 7 orders of magnitude attenuation. This diagnostic revealed that no significant changes of the focus quality are observed for low and high energy regimes, indicating that the triggered plasma has minimal impact on the DPM telescope system's focusing optical properties. Employing this diagnostic, the total reflectivity of the DPM telescope system was also characterized, measuring an average value of 68%. These results evidence an approximately 8.2 times increase in peak intensity at the focal plane compared to setup lacking the DPM system, which was achieved without requiring costly or time-intensive modifications to the large aperture focusing optics of the 10 PW laser beam delivery line.

Additionally, to characterize the temporal intensity contrast at the focal plane, dedicated laser interactions with ultrathin planar targets were performed using the DPM telescope system and compared to a system with silver-coated mirrors (otherwise identical to the DPM system), resulting in proton acceleration with a cut-off energy of  $>50$  MeV and  $\sim 15$  MeV, respectively. Besides, the laser-to-proton energy conversion efficiency increased by more than an order of magnitude when the DPM system was used. These findings therefore highlight that the temporal intensity contrast is significantly enhanced after reflection from the DPM telescope system compared to the intrinsic laser contrast, thereby enabling efficient laser-energy coupling with irradiated targets.

The implemented DPM telescope system offers relatively low-cost intensity adjustability and contrast enhancement of a multi-PW laser beam, while maintaining low aberrations at the focal plane and low sensitivity to misalignment. The validity of this system, combined with the ease of producing spherical optics in large quantities, sets thus a benchmark for expanding the capabilities of Terawatt to multi-PW laser facilities to achieve higher intensities without altering the beamline optics while enabling the exploration of more extreme laser-plasma conditions for applications that require ultra-high temporal contrast and intensity, particularly in cases involving ultrathin, near-critical density, or nanostructured targets.

## 5. Experimental details

The Extreme Light Infrastructure – Nuclear Physics (ELI-NP) laser facility recently demonstrated production of 10 PW pulses [33]. A detailed description of the high-power laser system (HPLS) architecture is given by Lureau *et al.* [37]. At the facility, two laser beam transport lines provide two different intensity regimes using long and short focal configurations. In this way, two experimental conditions are available for users: reaching up to  $10^{23}$  W/cm<sup>2</sup> for solid targets at the short-focal-length interaction chamber and  $\sim 10^{20}$  W/cm<sup>2</sup> for gas phase targets in the long-focal-length interaction chamber. An intermediate of  $\sim 10^{21}$  W/cm<sup>2</sup> intensity with a large area (and corresponding long Rayleigh length), smooth focal spot was required for investigating particle acceleration from solid targets (manuscript in preparation). Consequently, this investigation has been performed at the long-focal-length chamber with the intensity boost by the DPM system.

The DPM setup consists of eleven plasma mirror pairs installed on a compact (40 cm diameter) wheel, which permits a facile exchange between the shots on target (see Section 3 of SI for a mechanical drawing) without breaking the vacuum in the target chamber. Baffles are added between the pairs to screen the unused mirror pairs from ablated material upon interaction of the laser with the glass substrate. An investigation into the material sputtering on the plasma mirrors is given in Section 2.6 of SI.

The laser energy has been measured at a laser diagnostic bench using leakage from the compressor mirror. The pulse duration is measured with a FROG setup on-shot at the experimental chamber (see Section 6 of SI).

Ashland (<https://www.ashland.com>) GafChromic HD-V2 and EBT3 films, were used in the RCF detector.

**Funding.** Marvel Fusion GmbH; European Regional Development Fund (1/07.07.2016, COP, ID 1334); Ministerul Cercetării, Inovării și Digitalizării (PN23210105); Ministerul Cercetării, Inovării și Digitalizării (IOSIN funds); Charles University (GAUK 208123); Thales LAS France.

### Acknowledgments.

Jens Hartmann is acknowledged for microscope design and fruitful discussions. Daniel Popa and Bogdan Tatulea are acknowledged for technical support.

Extreme Light Infrastructure Nuclear Physics (ELI-NP) team acknowledge the support of the Romanian Government and the European Union through the European Regional Development Fund - the Competitiveness Operational Programme (1/07.07.2016, COP, ID 1334), and the Romanian Ministry of Research, Innovation and Digitalization: PN23210105 (Phase 2, the Program Nucleu). Accessing the ELI-NP facility is supported by the IOSIN

funds for research infrastructures of national interest funded by the Romanian Ministry of Research, Innovation and Digitalization.

M.T. thanks the support of Charles University through Student Grant No. GAUK 208123.

**Disclosures.** V.S., M.Sp., A.F., B.G.-I., J.J.B., C.B., G.B., A.F.B., A.C., J.D'M, F.D., M.E., D.G., M.M.G., O.J., K.K., S.K., M.M.-P., N.P., H.R., E.S., M.St., Sv.S., A.U., E.G., D.E.R., M.Sc., G.K.: Marvel Fusion GmbH (I,E). H.R.: Marvel Fusion GmbH (C,S), A.A., O.C., C.D.: Thales LAS France (E). V.S., M.Sp., B.G.-I., E.G., D.E.R., M.Sc., G.K.: Marvel Fusion GmbH (P).

**Data availability.** Data underlying the results presented in this paper are not publicly available at this time but may be obtained from the authors upon reasonable request.

**Supplemental document.** Supplementary materials are available free of charge on the journal website.

## References

1. A. Macchi, M. Borghesi, and M. Passoni, "Ion acceleration by superintense laser-plasma interaction," *Reviews of Modern Physics* **85**, 751-793 (2013).
2. J. H. Bin, W. J. Ma, H. Y. Wang, et al., "Ion Acceleration Using Relativistic Pulse Shaping in Near-Critical-Density Plasmas," *Physical Review Letters* **115**, 064801 (2015).
3. J. H. Bin, M. Yeung, Z. Gong, et al., "Enhanced Laser-Driven Ion Acceleration by Superponderomotive Electrons Generated from Near-Critical-Density Plasma," *Physical Review Letters* **120**, 074801 (2018).
4. T. Tajima, X. Q. Yan, and T. Ebisuzaki, "Wakefield acceleration," *Reviews of Modern Plasma Physics* **4**, 7 (2020).
5. C. Danson, D. Hillier, N. Hopps, et al., "Petawatt class lasers worldwide," *High Power Laser Science and Engineering* **3**, e3 (2015).
6. H. Ruhl and G. Korn, "Uniform volume heating of mixed fuels within the ICF paradigm," (2023).
7. M. M. Murnane, H. C. Kapteyn, and R. W. Falcone, "High-Density Plasmas Produced by Ultrafast Laser Pulses," *Physical Review Letters* **62**, 155-158 (1989).
8. D. M. Gold, H. Nathel, P. R. Bolton, et al., "Prepulse suppression using a self-induced ultrashort pulse plasma mirror," in *Proc.SPIE*, 1991), 41-52.
9. H. C. Kapteyn, M. M. Murnane, A. Szoke, et al., "Prepulse energy suppression for high-energy ultrashort pulses using self-induced plasma shuttering," *Opt Lett* **16**, 490-492 (1991).
10. C. Ziener, P. S. Foster, E. J. Divall, et al., "Specular reflectivity of plasma mirrors as a function of intensity, pulse duration, and angle of incidence," *Journal of Applied Physics* **93**, 768-770 (2003).
11. T. Wittmann, J. P. Geindre, P. Audebert, et al., "Towards ultrahigh-contrast ultraintense laser pulses-complete characterization of a double plasma-mirror pulse cleaner," *Review of Scientific Instruments* **77**(2006).
12. A. Levy, T. Ceccotti, P. D'Oliveira, et al., "Double plasma mirror for ultrahigh temporal contrast ultraintense laser pulses," *Opt Lett* **32**, 310-312 (2007).
13. C. Thaur, F. Quere, J. P. Geindre, et al., "Plasma mirrors for ultrahigh-intensity optics," *Nature Physics* **3**, 424-429 (2007).
14. T. Sokollik, S. Shiraishi, J. Osterhoff, et al., "Tape-drive Based Plasma Mirror," *AIP Conference Proceedings* **1299**, 233-237 (2010).
15. C. Rödel, M. Heyer, M. Behmke, et al., "High repetition rate plasma mirror for temporal contrast enhancement of terawatt femtosecond laser pulses by three orders of magnitude," *Applied Physics B* **103**, 295-302 (2011).
16. J. Braenzel, A. Andreev, M. Schnuerer, et al., "Sub-structure of laser generated harmonics reveals plasma dynamics of a relativistically oscillating mirror," *Physics of Plasmas* **20**(2013).
17. J. S. Green, N. P. Dover, M. Borghesi, et al., "Enhanced proton beam collimation in the ultra-intense short pulse regime," *Plasma Physics and Controlled Fusion* **56**, 084001 (2014).
18. G. G. Scott, V. Bagnoud, C. Brabetz, et al., "Optimization of plasma mirror reflectivity and optical quality using double laser pulses," *New Journal of Physics* **17**, 033027 (2015).
19. P. L. Poole, A. Krygier, G. E. Cochran, et al., "Experiment and simulation of novel liquid crystal plasma mirrors for high contrast, intense laser pulses," *Scientific Reports* **6**(2016).
20. B. H. Shaw, S. Steinke, J. van Tilborg, et al., "Reflectance characterization of tape-based plasma mirrors," *Physics of Plasmas* **23**(2016).
21. M. Speicher, D. Haffa, M. A. O. Haug, et al., "Integrated double-plasma-mirror targets for contrast enhancement in laser ion acceleration," *Journal of Physics: Conference Series* **1079**(2018).
22. A. Zingale, S. Steinke, J. Bin, et al., "Sustainable High Repetition Rate Plasma Mirrors for Petawatt Lasers," in *APS Meeting Abstracts*, 2018).
23. N. A. Czapl, "High Throughput and Contrast Enhancement from Ultrathin Liquid Crystal Films in a Double Plasma Mirror Configuration," *Bulletin of the American Physical Society*, PO03.00007 (2020).
24. I. W. Choi, C. Jeon, S. G. Lee, et al., "Highly efficient double plasma mirror producing ultrahigh-contrast multi-petawatt laser pulses," *Opt Lett* **45**, 6342-6345 (2020).
25. N. P. Dover, T. Ziegler, S. Assenbaum, et al., "Enhanced ion acceleration from transparency-driven foils demonstrated at two ultraintense laser facilities," *Light: Science & Applications* **12**, 71 (2023).
26. M. Nakatsutsumi, A. Kon, S. Buffechoux, et al., "Fast focusing of short-pulse lasers by innovative plasma optics toward extreme intensity," *Opt Lett* **35**, 2314-2316 (2010).
27. M. Nakatsutsumi, Y. Sentoku, A. Korzhimanov, et al., "Self-generated surface magnetic fields inhibit laser-driven sheath acceleration of high-energy protons," *Nat Commun* **9**, 280 (2018).
28. R. Wilson, M. King, R. J. Gray, et al., "Development of Focusing Plasma Mirrors for Ultraintense Laser-Driven Particle and Radiation Sources," *Quantum Beam Science* **2**, 1 (2018).
29. S. Kojima, Y. Abe, E. Miura, et al., "Demonstration of a spherical plasma mirror for the counter-propagating kilojoule-class petawatt LFEX laser system," *Opt. Express* **30**, 43491-43502 (2022).
30. X. Geng, T. Xu, L. Zhang, et al., "Compact laser wakefield acceleration toward high energy with micro-plasma parabola," *Matter and Radiation at Extremes* **9**(2024).
31. A. S. Kutter, *Der Schiefspiegler* (Sky Publ. Corp., Cambridge, Massachusetts, 1953).

- 32. R. A. Buchroeder, "Tilted-Component Telescopes. Part I: Theory," *Applied Optics* **9**, 2169-2171 (1970).
- 33. C. Radier, O. Chalus, M. Charbonneau, et al., "10 PW peak power femtosecond laser pulses at ELI-NP," *High Power Laser Science and Engineering* **10**, e21 (2022).
- 34. Y. Nomura, L. Veisz, K. Schmid, et al., "Time-resolved reflectivity measurements on a plasma mirror with few-cycle laser pulses," *New Journal of Physics* **9**, 9 (2007).
- 35. O. Chalus, C. Derycke, M. Charbonneau, et al., "High contrast 10 PW laser system at ELI-NP," submitted (2024).
- 36. B. Gonzalez-Izquierdo, P. Fischer, M. Touati, et al., "Efficient laser-driven proton acceleration from a petawatt contrast-enhanced second harmonic mixed-glass laser system," *Physics of Plasmas* **31**(2024).
- 37. F. Lureau, G. Matras, O. Chalus, et al., "High-energy hybrid femtosecond laser system demonstrating  $2 \times 10$  PW capability," *High Power Laser Science and Engineering* **8**, e43 (2020).